HAL
open science

# Seasonal and magnetic activity variations of ionospheric electric fields above the southern mid-latitude station, Bundoora, Australia

M. L. Parkinson, R. Polglase, B. G. Fejer, L. Scherliess, P. L. Dyson, S. M. Ujmaia

## To cite this version:

M. L. Parkinson, R. Polglase, B. G. Fejer, L. Scherliess, P. L. Dyson, et al.. Seasonal and magnetic activity variations of ionospheric electric fields above the southern mid-latitude station, Bundoora, Australia. Annales Geophysicae, 2001, 19 (5), pp.521-532. hal-00316843

**HAL Id: hal-00316843**

**https://hal.science/hal-00316843v1**

Submitted on 18 Jun 2008

**HAL** is a multi-disciplinary open access archive for the deposit and dissemination of scientific research documents, whether they are published or not. The documents may come from teaching and research institutions in France or abroad, or from public or private research centers.

L'archive ouverte pluridisciplinaire **HAL**, est destinée au dépôt et à la diffusion de documents scientifiques de niveau recherche, publiés ou non, émanant des établissements d'enseignement et de recherche français ou étrangers, des laboratoires publics ou privés.

Annales Geophysicae (2001) 19: 521–532 © European Geophysical Society 2001

Annales Geophysicae

# Seasonal and magnetic activity variations of ionospheric electric fields above the southern mid-latitude station, Bundoora, Australia

**M. L. Parkinson[1], R. Polglase[1], B. G. Fejer[2], L. Scherliess[2], P. L. Dyson[1], and S. M. Ujmaia[1]**

[1]Department of Physics, La Trobe University, Melbourne, Victoria 3086, Australia
[2]Center for Atmospheric and Space Sciences, Utah State University, Logan, UT 84322–4405, USA

Received: 16 November 2000 – Revised: 19 March 2001 – Accepted: 23 March 2001

**Abstract.** We investigate the seasonal, local solar time, and geomagnetic activity variations of the average Doppler velocity measured by an HF digital ionosonde deployed at Bundoora, Australia (145.1° E, 37.7° S, geographic; 49° S magnetic). The Doppler velocities were heavily averaged to suppress the short-term effects (<3 hours) of atmospheric gravity waves, and thereby obtain the diurnal variations attributed to the tidally-driven ionospheric dynamo and electric fields generated by magnetic disturbances. The observed seasonal variations in Doppler velocity were probably controlled by variations in the lower thermospheric winds and ionospheric conductivity above Bundoora and in the magnetically conjugate location. The diurnal variations of the meridional (field-perpendicular) drifts and their perturbations exhibited a complex structure, and were generally smaller than the variations in the zonal drifts. The latter were basically strongly westward during the evening to early morning, and weakly eastward during the late morning to just past noon. The zonal perturbations were strongly enhanced by increasing geomagnetic activity, and closely resembled the perturbation drifts measured by the incoherent scatter radar (ISR) at Millstone Hill (71.5° W, 42.6° N; 57° N). There was also some resemblance between the diurnal variations in the meridional drifts. Overall, the comparisons suggest that with sufficient averaging, Doppler velocities measured with digital ionosondes at mid-latitudes correspond to true ion motions driven by ionospheric electric fields. This is a useful result because apart from the ISRs located in the American-European sector, there are no ground-based instruments capable of measuring electric fields in the mid-latitude ionosphere.

**Key words.** Ionosphere (electric fields and currents; ionosphere-atmosphere interactions; mid-latitude ionosphere)

## 1 Introduction

We need to understand the physics of electric fields manifesting in the mid-latitude ionosphere and thermosphere to fully describe the global atmospheric response to magnetic storms generated within the Sun. This entails understanding the penetration of magnetospheric and disturbance dynamo electric fields well into the low-latitude plasmasphere during geomagnetic storms (Fejer, 1997). It is also important to understand mid-latitude electric fields because they influence the height of the F-region ionosphere, which might be a sensitive indicator of global climate change in the troposphere (Roble and Dickinson, 1989; Jarvis et al., 1998). A key requirement of many studies is the availability of a reliable empirical model of mid-latitude electric fields (e.g. Wand, 1981; Buonsanto and Witasse, 1999; Scherliess et al., 2000).

The basic physics affecting electric fields observed at mid-latitudes are summarised as follows:

1. During geomagnetic quiet conditions, the ring current shields the plasmasphere from the magnetospheric electric fields driving steady-state convection.

2. Under these conditions, the electric fields at a mid-latitude station are dominated by the combined effect of the local and conjugate E-region dynamo driven by atmospheric tides. However, the electric field associated with a particular magnetic flux tube cannot be considered in isolation from the rest of the ionosphere and thermosphere.

3. The winds in the upper thermosphere must also be considered, especially during the nighttime, when the F-region conductivity becomes more important than the E-region conductivity (Du and Stening, 1999a).

4. Moreover, at all times, there must be short-term variability in the dynamo fields associated with irregular neutral winds. Perhaps this variability is driven by atmospheric gravity waves which might carry electric fields with them.

5. When the magnetospheric convection is non-steady, as is the case during a geomagnetic storm, there is a time delay for the ring current to readjust and thereby shield the plasmasphere from the large electric fields at high latitudes. Hence, immediately following the growth

*Correspondence to:* M. L. Parkinson
(m.parkinson@latrobe.edu.au)

phase of a substorm, there are short-lived (∼tens of minutes) "prompt penetration" electric fields of magnetospheric origin (Fejer and Scherliess, 1998).

6. The Joule heating dissipated during major geomagnetic storms will modify the global thermospheric wind circulation and also launch atmospheric gravity waves. When these disturbances propagate to mid-latitudes, they will produce longer lasting (∼hours) disturbance dynamo fields (Scherliess and Fejer, 1998).

Taken together, 5 and 6 constitute the "perturbation electric fields", but both contributions can be separated using a superimposed epoch analysis of time series data. Heelis and Coley (1992) used Dynamics Explorer-2 (DE-2) measurements to show how these perturbation electric fields are important down to 45° magnetic latitude, even during quiet times.

Considerable progress has been made in modelling the geomagnetic quiet and disturbance electric fields at equatorial and low latitudes (Richmond, 1995; Fejer, 1997; Du and Stening, 1999b). However, our knowledge of the thermospheric tides, winds, and ionospheric conductivity variations on a global scale is still incomplete, and modelling the plasmaspheric electric fields driven by the quiet time dynamo at mid-latitudes remains a challenging problem. Moreover, empirical models of mid-latitude electric fields suffer from limited data sets recorded by a few incoherent scatter radars (ISRs) concentrated in the American-European sector, and intermittent satellite measurements made in other regions of geospace (Parkinson et al., 2000).

Continuous, global measurement of low- and mid-latitude electric fields is constrained by the availability of ISRs and satellites. For example, ISRs may only operate in the required mode for a few days per month because of the high operational cost, and obviously satellites are very expensive to launch and have a finite lifetime because of atmospheric drag, amongst other factors. Thus, it would be useful to demonstrate if Doppler-velocity measurements made with digital ionosondes represent an economical ground-based method of making long-term ionospheric electric field measurements at mid-latitudes. Hence, an important goal of our research group is to validate the interpretation of digital ionosonde measurements via comparisons with the results of other instruments and models.

In this study, we compile a 12-month database of Doppler-velocity measurements made with a Digital Portable Sounder 4 ("Digisonde" hereafter) (Haines and Reinisch, 1995; Reinisch et al., 1997) installed at Bundoora, Melbourne (145.1° E, 37.7° S, geographic; 49° S geomagnetic). The velocities are assumed to correspond to true F-region ion drifts driven by ionospheric electric fields for the purpose of this analysis, and are compared with other empirical representations of mid-latitude electric fields (e.g. Buonsanto and Witasse, 1999; Scherliess et al., 2000). Despite limitations in our measurements (as with other techniques), the comparisons are promising.

## 2 Digisonde operation and database

The Doppler-velocity technique employed by the Digisonde has been described in detail elsewhere (Reinisch, 1986; Wright and Pitteway, 1994; Scali et al., 1995a; Parkinson et al., 1997a). Here we give a brief description of the technique and address problems related to our database. The overhead ionosphere is illuminated with a broad (∼60°), pulsed (∼100 Hz), HF radio beam emitted by a 22 m tall crossed vertical delta antenna. The DPS-4 transmitter pulses have a peak power level of 300 W and a half-power bandwidth of 60 kHz. Total reflection echoes from the ionosphere are received by a triangular antenna array consisting of four crossed loop antennas (with one in the centre), each 1.5 m in diameter and with a nearly isotropic sensitivity across the radar bandwidth. There must be at least three non-colinear antenna elements to resolve the angle-of-arrival (AOA) and Doppler shifts of echoes in the $x$, $y$, and $z$ directions. By phasing alternate arms of the transmitter and crossed loop antennas by $\pm\pi/2$ radians, discrimination between the ordinary and extraordinary modes of polarisation is achieved. The received waveforms are compared with a very stable clock (local oscillator) to record independent time series of in-phase and quadrature samples received on each antenna. The length of the time series, or the integration time, is changed depending on the objective of the experiment, and may range anywhere from between a fraction of a second to 2 minutes.

During the integration time, there may be echoes from several ionospheric irregularities, so that attempts to "triangulate" the AOA of an echo using the relative phases of signals recorded across the antenna array may produce erroneous results, i.e. the instantaneous phases measured on the receiving array may be caused by the superposition of a number of plane wave fronts arriving from different directions. However, assuming that each echo has a slightly different and resolvable Doppler shift, this problem is circumvented by first Fourier transforming the time series into the Doppler frequency domain, and then separately calculating the AOA of each signal sorted into separate Doppler bins. Hence, a "skymap" showing the AOAs and corresponding Doppler shifts for an ensemble of echoes is formed by analysing the spectra resulting from a succession of time series. When the Doppler shift and AOA of at least three widely separated echoes has been measured, a least squares analysis can be performed to infer the optimum 3-dimensional velocity explaining the observed Doppler shifts. The accuracy of the velocity estimates improves with the number of echoes detected per unit time. In this way, the bulk motion of the ionosphere above the station can be reliably determined.

The choice of the integration time, $\Delta T$, is constrained by the time-bandwidth product, $\Delta T \Delta f = 1$. Hence, there is a trade-off between locating the echoes in time and locating them in Doppler frequency. If the integration time is too short, the spectral resolution will be too coarse to resolve all the echoes in the Doppler domain. Conversely, if the integration time is longer than the finite lifetime of the ionospheric irregularities (<2 min), then information will be lost. Fur-

thermore, in practice, the integration time is increased by decreasing the sampling rate. Hence, the Nyquist frequency may become too low, causing the Doppler shift and AOA of echoes to alias. Experience indicates that an integration time of about 40.96 sec and a Nyquist frequency of $>1.5$ Hz are suitable for measuring the line-of-sight Doppler motions of $\sim 40\ \mathrm{m\,s^{-1}}$ associated with electric fields and gravity waves at mid-latitudes, without causing too much aliasing during intervals of unusually strong flow.

Other studies suggest that Digisonde measurements of F-region motion agree with true ion drifts at high latitudes (e.g. Cannon, 1991; Grant et al., 1995; Smith et al., 1998). However, comparisons between time series of Digisonde and ISR measurements indicate the agreement becomes worse with decreasing latitude (Scali et al., 1997). The poor agreement found in some studies might be partly due to the difficulty of obtaining measurements made using the same sampling times and volumes. Nevertheless, Digisonde observations of the relatively small dynamo drifts at low latitudes must sometimes be swamped by Doppler shifts caused by production and loss processes (Bittencourt and Abdu, 1981). Moreover, the motion of reflection surfaces (From et al., 1988) at the phase velocity of atmospheric gravity waves is always a concern. In this study, we heavily average the Doppler velocities to remove short-term variability associated with the latter effect.

Here we compile all the Digisonde measurements made at Bundoora on 316 days during the 12 month interval 11 March 1999 to 29 February 2000. Doppler-velocity measurements were made using a 20.48 sec integration time in the "Dopplionogram" mode (Parkinson et al., 1999) during 11 March to 19 August 1999 (days 98 to 231). A Dopplionogram is simply a digital ionogram with high-resolution Doppler shifts recorded during the frequency scan. We initially chose this mode to minimise interference with other users of the HF spectrum. After August 19 all measurements were made using a 40.96 sec integration time on our licensed fixed frequencies of 5.48 MHz during the "daytime" (7 am to 7 pm) and 3.40 MHz during the "nighttime" to further mitigate interference problems, whilst also enhancing the Doppler resolution. One velocity vector was calculated using all the echoes recorded during a single integration time, irrespective of the mode of operation.

The chosen fixed frequencies were important because $f_{\min}$ and $f_0$F2 change with the season and sunspot cycle, as well as diurnally. For example, in Fig. 1c, we will see the daytime velocities appear somewhat larger partly because often, no measurements were obtained during the night when $f_{\min}$ exceeded 3.40 MHz due to absorption, or $f_0$F2 dropped beneath 3.40 MHz due to the arrival of the mid-latitude ionospheric trough. Sometimes the chosen frequencies also resulted in the detection of E-region echoes and Doppler shifts instead. However, so far the Bundoora measurements have not revealed the persistent vertical gradients in horizontal velocity found in the polar cap (Parkinson et al., 1997b). Nevertheless, any echoes recorded at group ranges less than 180 km were rejected in the present analysis.

The Doppler velocities measured using the fixed-frequency mode were, on average, a factor of 1.5 times larger than those measured using the Dopplionogram mode (but they had the same basic directions). This is because the velocity vectors were averaged with respect to time in the fixed-frequency mode, whereas the velocity vectors were averaged with respect to time and frequency (i.e. group height) in the frequency-scanning mode. We argue that the smaller velocity magnitudes measured in the frequency-scanning mode were more representative of the true bulk motion of the ionosphere because they were the vector average of motions over all heights in the bottom-side ionosphere. Hence, we normalised the velocities recorded in the fixed-frequency mode to the magnitude of the velocities recorded in the Dopplionogram mode. However, we caution that, as with other techniques used to measure ionospheric electric fields, the relative variations in our measurements have greater accuracy than the absolute values.

Data recorded during 11 March 1999 to 29 February 2000 were chosen for this study because they contain measurements with the least number of instrumental problems during four consecutive, distinct seasons (autumn, winter, spring, and summer). The Doppler spectra generated in real time by the radar were processed using the standard Drift Data Analysis (DDA) software developed by the University of Massachusetts Lowell Center for Atmospheric Research (Scali et al., 1995b). DDA calculates Doppler velocities in the Cartesian geographic reference frame of the receiving antenna array. The database obtained is summarised by Fig. 1 which shows the decimetric (10.7-cm) solar flux and *Kp* index ($\times 10$) (part a), and contour plots of the vertical velocity (part b), and the magnitude of the horizontal velocity (part c). The abscissa is modified day number where day one is 1 January 1999, and day 366 is 1 January 2000, and the ordinate is local solar time (LST = UT + 09 h 40 m). The velocity components for each day were averaged over 15 min bins of LST. The vertical green and black strips in Fig. 1b and c, respectively, correspond to outages due to equipment failures (e.g. during days 126 to 153). The azimuths of the horizontal velocities are not shown because of their difficult interpretation in this format.

Figure 1a shows that solar activity was approaching sunspot maximum levels throughout the study period. Although the solar activity was somewhat lower during austral autumn, it will be years before our database is large enough to sustain sorting according to season and solar flux level. The average solar flux index, sunspot number, and *Kp* index during the study period were 159, 99, and 2.3, respectively.

A striking feature of Fig. 1b is the sharp downward (dark blue) and weaker upward (brown) vertical motions associated with F-region sunrise and sunset, respectively. These motions are partly "illusions" created by the dominance of production (sunrise) and loss (sunset) of ionisation in the lower F region. As expected, the signatures of sunrise and sunset are widely separated in LST near the summer solstice (day 355), yet closely separated near winter solstice (day 172). The detection of these velocity enhancements partly

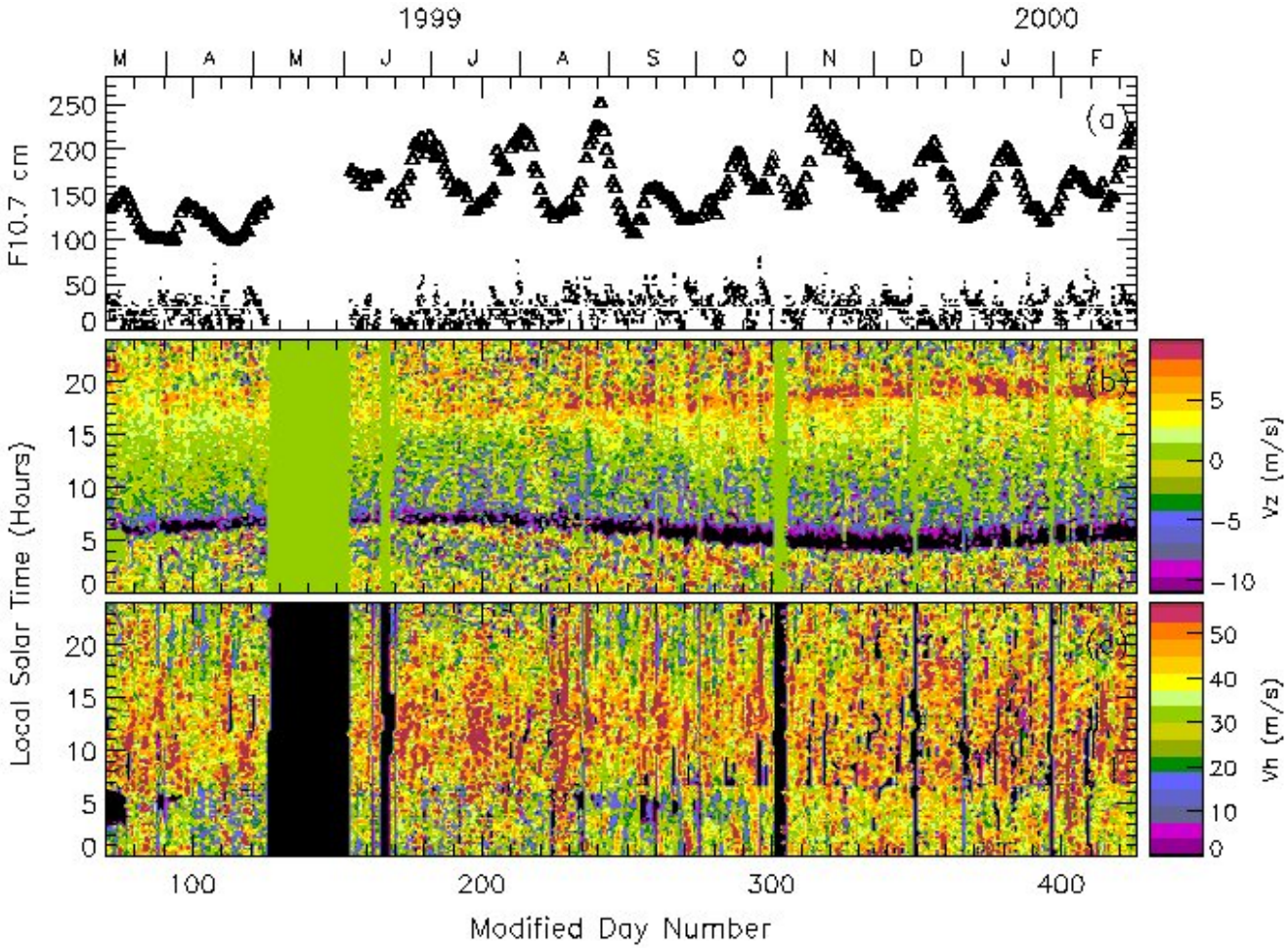


**Fig. 1.** Summary plot of the database analysed in this paper. **(a)** Decimetric (10.7-cm) solar flux (triangles) and the *Kp* index (×10) (dots), both versus modified day number with day 1 commencing on 1 January 1999. **(b)** Contour plot of the vertical component of Doppler-velocity averaged in 15 min bins of LST and 1 day bins of day number. **(c)** The same as (b) except for the magnitude of the horizontal velocity. Tick marks on the abscissa are at 10 day intervals.

validates correct operation of the Digisonde and data analysis software.

Moreover, we routinely calibrated the phase response of the antenna array to eliminate systematic errors in the AOA of echoes, and hence, the calculated velocities. In addition, we always interleaved routine 2 min auto-scaleable ionograms at 10 min intervals to provide basic ionospheric parameters and to help validate the Doppler-velocity measurements.

Figure 1c shows that the magnitude of the horizontal velocity varied between about 15 and 60 m s$^{-1}$ throughout the study period. The validity of the adopted normalisation procedure is also demonstrated because the magnitude of the horizontal velocities were similar throughout the study period, when the large day-to-day variability was excluded.

## 3 Digisonde observations

In this section, we illustrate the intrinsic variability of the Doppler velocity measurements, and the problems with transforming them into a magnetic reference frame. Figure 2 shows mass plots of the number of velocities for different components measured during September 1999. Parts a to c show the velocity components in the Cartesian reference frame of the receiver antenna array after sorting them into bins of 15 min in LST. Although there is a lot of scatter in the vertical velocity component (part a), it averages out to be close to zero (0.5 m s$^{-1}$) over the entire day. The diurnal variation is consistent with the expected changes in the height of the F region, namely decreasing from sunrise to just past local noon, and thereafter increasing. The horizontal velocities (part b) have mode values that vary between about 20 and 40 m s$^{-1}$, with a distinct maximum just past local noon that may be related to the enhancements of daytime ionospheric conductivity. The velocity directions (part c) exhibit strong evidence for a diurnal tide of some kind.

The velocity components measured in the Cartesian reference frame were transformed into components in the magnetic reference frame by making use of the standard assump-

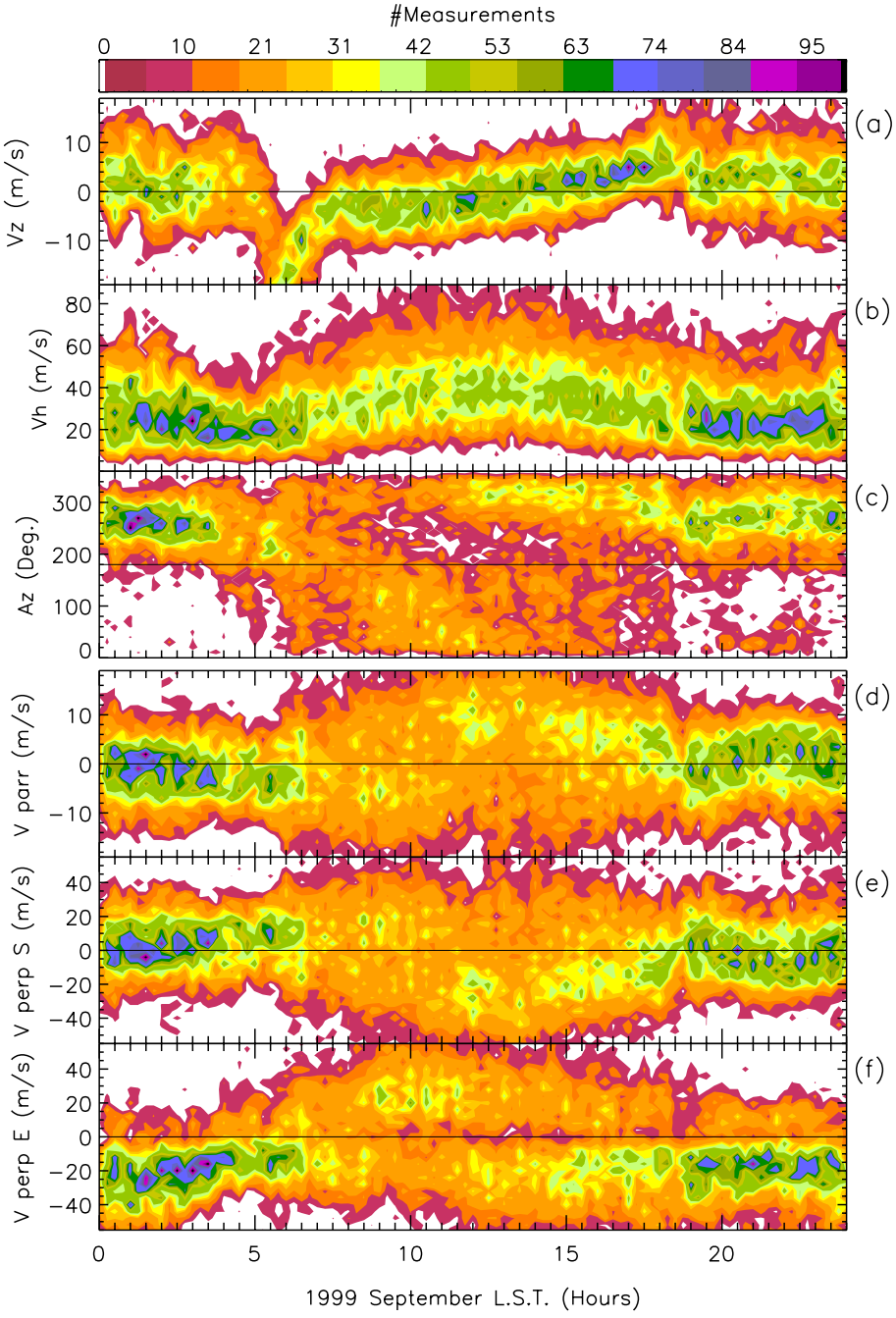


**Fig. 2.** Mass plot of 56159 independent Doppler velocities measured using a 40.96 sec integration time during September 1999. The colour scale at the top gives the number of velocities found in each bin of 15 min in LST and using small bin sizes for each velocity component. **(a)** The vertical velocity component, $V_z$, using a bin size of 2 m s$^{-1}$. **(b)** The horizontal velocity, $V_h$, using a bin size of 5 m s$^{-1}$. **(c)** The azimuth of the horizontal velocity, $Az$, using a bin size of 10°. **(d)** The field-aligned velocity, $V_\parallel$, using a bin size of 2 m s$^{-1}$. **(e)** The field-perpendicular southward velocity, $V_{\perp S}$, using a bin size of 5 m s$^{-1}$. **(f)** The field-perpendicular eastward velocity, $V_{\perp E}$, using a bin size of 5 m s$^{-1}$. Tick marks on the abscissa are at 30 min intervals.

tion of $\boldsymbol{E} \times \boldsymbol{B}/B^2$ drift in the F region. Figure 2d shows that the field-aligned motion $V_\parallel$ was predominantly upward during 1000 to 1800 LST, and probably also during the early evening. $V_\parallel$ was predominantly downward during the early morning. Our drift observations are of the bottom-side ionosphere where the combined effect of ion diffusion and coupling to the neutral wind must be considered. The meridional winds above Millstone Hill (Buonsanto and Witasse, 1999) and probably Bundoora (Dyson et al., 1997) are basically poleward during the day and equatorward during the night, which has limited agreement with the wind directions directly implied by the variation of $V_\parallel$ at Bundoora. Hence, the effects of diffusion must also influence $V_\parallel$. The diurnal variation shown in Fig. 2d is partly consistent with an F-region ionosphere that fills the plasmasphere during the daytime, and then is replenished by the plasmasphere during the night (Saxton et al., 1989). In a future study, we will resolve the relative importance of the two mechanisms, deriving the meridional neutral winds at Bundoora using $V_\parallel$, the electron density profiles derived from concurrent ionograms, and the standard method of compensating for diffusion employed in the analysis of ISR measurements (Buonsanto and Witasse, 1999).

Figure 2e,f shows the two orthogonal components of the

drift in a plane perpendicular to the magnetic field, namely the southward ($V_{\perp S}$) and eastward ($V_{\perp E}$) drift, respectively. $V_{\perp S}$ is basically equatorward (downward) during the day and poleward (upward) during the early morning. However, it is only partly consistent with the diurnal variation of the F-region height implied by part a. $V_{\perp S}$ is nearly a mirror image of $V_{\parallel}$, which is seen by comparing Fig. 2d,e. The mirroring of $V_{\perp S}$ and $V_{\parallel}$ is a well-known consequence of coupling between the neutral wind and ion drift (Behnke and Harper, 1973), and implies partial control of $V_{\parallel}$ by variability in the thermospheric winds.

On the other hand, the zonal drifts are electrically driven, and distinctly westward except briefly during the day (especially between 0900 to 1200 LST).

Note that $V_{\perp S}$ is equivalent to the zonal electric field, $E_{\perp E}$, and $V_{\perp E}$ is equivalent to the equatorward electric field, $E_{\perp N}$, when allowing for the scaling $1\ \mathrm{mV\,m^{-1}} \equiv 18.3\ \mathrm{m\,s^{-1}}$ applicable to the geomagnetic field above Bundoora. Our drift measurements imply that electric field strengths of 1–3 $\mathrm{mV\,m^{-1}}$ are common at the magnetic latitude of Bundoora (49° S).

Fortunately, the enhancements in $V_z$ due to photochemistry at sunrise and sunset, shown in Fig. 2a, only have a limited effect on the estimated velocity components in the magnetic reference frame. This is revealed by an analysis of the standard equations transforming the velocities:

$$V_{\parallel} = V_h \cos Az \cos I + V_z \sin I \quad (1)$$

$$V_{\perp S} = V_z \cos I - V_h \cos Az \sin I \quad (2)$$

$$V_{\perp E} = V_h \sin Az \quad (3)$$

where $I = 69°$ is the dip angle at Bundoora. We note that:

1. The zonal drift $V_{\perp E}$ is not at all affected by $V_z$, and hence, it is the most accurate component.
2. The meridional drift $V_{\perp S}$ is primarily affected by $V_h$ because $V_h$ is usually $> V_z$ and $\sin I > \cos I$.
3. The field-aligned drift $V_{\parallel}$ is frequently primarily affected by $V_h$ because $V_h$ is usually $> V_z$, and this tends to dominate over the effect of $\sin I > \cos I$.
4. However, $V_{\perp S}$ and $V_{\parallel}$ are completely determined by $V_z$ when the drift direction is zonal, so caution is still necessary, especially near sunrise and sunset.

Overall, the effects of photochemistry are limited at our mid-latitude station and we note that most of the features to be presented in the following section persist even when we set $V_z = 0$ prior to transforming the velocities to the magnetic reference frame.

As an aside, the situation is somewhat different at an equatorial station where $V_{\perp S}$ is always completely determined by $V_z$. However, $V_{\parallel}$ and $V_{\perp E}$ are never affected by $V_z$. Lastly, at a polar cap station, $V_{\parallel}$ is always completely determined by $V_z$, whereas $V_{\perp S}$ and $V_{\perp E}$ are never affected by $V_z$. Thus, estimates of field-perpendicular electric fields using Digisondes are least affected by diffusion and photochemistry at a polar cap station.

## 4 Results and discussion

In this section, we investigate the detailed variations of drift velocity with season and LST. Figures 3 to 7 show the results for summer (December, January, February), autumn (March, April, May), winter (June, July, August), spring (September, October, November), and for all seasons combined, respectively. Parts a and b of each figure show the average diurnal variation in the velocity components $V_{\perp S}$ and $V_{\perp E}$, respectively. Prior to averaging, the data were sorted into 15 min bins and two broad categories of *Kp*, namely quiet to moderately disturbed ($Kp < 3$; bold dots) and disturbed ($Kp \geq 3$; triangles). Hence, the perturbation drifts given by the differences between velocities for the two categories are shown in parts c and d, respectively.

First consider Fig. 3, the drift velocities and their perturbations for summer. In each of the two categories of magnetic disturbance, the average *Kp* values were 1.5 and 3.7, the average 10.7-cm solar flux indices were 166 and 158, and the number of independent velocities were 60982 and 33189, respectively. $V_{\perp S}$ was basically poleward for all LST, with evidence for a weak enhancement near ∼07 h and a stronger enhancement near ∼16 h LST. The perturbations in $V_{\perp S}$ (part c) were weak and showed a lot of scatter during the day. These fluctuations were partly significant because they were merely indicative of the particular geomagnetic storms occurring during the chosen summer interval.

On the other hand, $V_{\perp E}$ (part b) and its perturbations (part d), show some distinctive, reproducible features. $V_{\perp E}$ was eastward during the morning (∼05–11 h) and late afternoon (∼15–18 h), though otherwise westward, especially during the night. The daytime perturbations in $V_{\perp E}$ were variable, but they clearly trended toward westward during the night.

Figure 4 shows the drift velocities and their perturbations for autumn when the solar flux was somewhat lower than during other seasons. Few good observations were obtained during May, but the statistics are still fairly good. In each of the two categories of magnetic disturbance, the average *Kp* values were 1.5 and 3.7, the average 10.7-cm solar flux indices were 122 and 122, and the number of independent velocities were 30871 and 10247, respectively. Again, $V_{\perp S}$ was the weaker component but it was sometimes equatorward during autumn, especially near ∼12 h, 17–18 h, and 21–02 h. Again, the perturbations in $V_{\perp S}$ were weak, showing a lot of scatter. $V_{\perp E}$ during the autumn resembled $V_{\perp E}$ during the summer, having eastward enhancements near ∼5 h and 10 h, but the secondary enhancement in the late afternoon (∼15–18 h) was subdued. Overall, $V_{\perp E}$ had become more westward, though again, especially during the night. The perturbations in $V_{\perp E}$ showed substantial scatter, but they tended to be eastward during the morning and westward during the afternoon and evening.

Figure 5 shows some very well defined trends in the drift velocities and their perturbations for winter. In each of the two categories of magnetic disturbance, the average *Kp* values were 1.4 and 3.8, the average 10.7-cm solar flux indices were 175 and 184, and the number of independent velocities

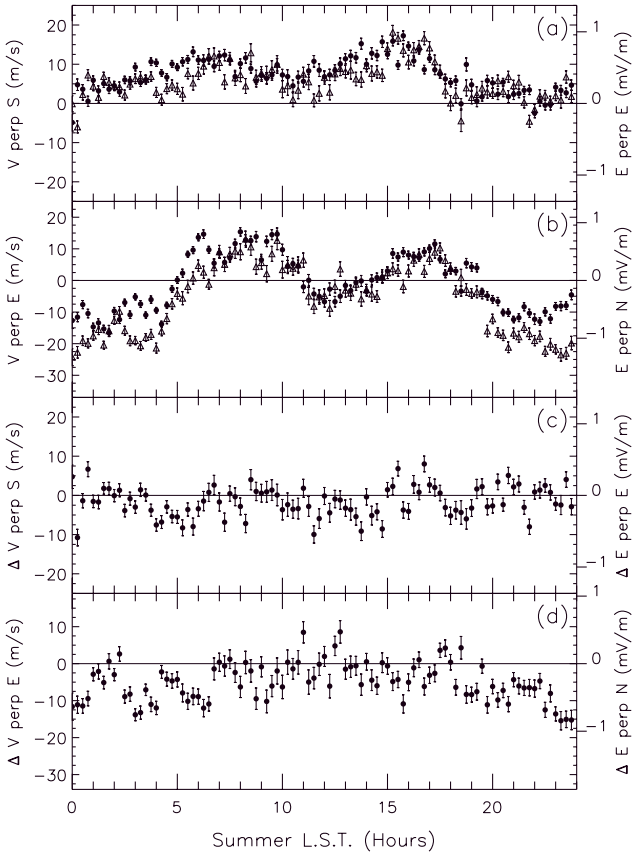


**Fig. 3.** The summer average diurnal variation of **(a)** the Doppler-velocity component $V_{\perp S}$ and **(b)** the component $V_{\perp E}$. The bold dots are drifts for $Kp < 3$ and the triangles are drifts for $Kp \geq 3$. The corresponding perturbation drifts are shown in **(c)** for $V_{\perp S}$ and in **(d)** for $V_{\perp E}$. The error bars are standard deviations of the means. Equivalent electric field strengths are shown at right, and tick marks on the abscissa are at 1 hour intervals.

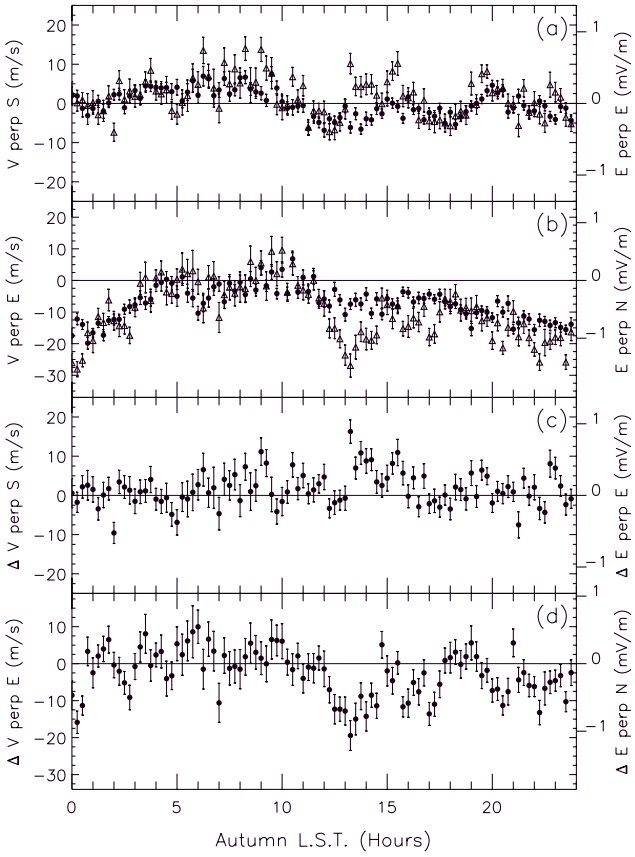


**Fig. 4.** The same results as Fig. 3 except for autumn.

were 44006 and 19457, respectively. $V_{\perp S}$ was strongly equatorward during the daytime, ∼10–18 h, and weakly equatorward during ∼21–23 h. Otherwise, $V_{\perp S}$ was persistently poleward, especially during ∼01–09 h, and briefly after sunset (∼19–21 h). The corresponding perturbation drifts still show a lot of scatter. $V_{\perp E}$ was clearly eastward during the daytime (∼08–14 h), and strongly westward during the late afternoon, evening, and morning. The corresponding perturbation drifts were clearly westward as well, except for a few brief periods during the daytime. Similar behaviour in the quiet zonal drifts above Millstone Hill was originally described by Wand and Evans (1981a).

Figure 6 shows the drift velocities and their perturbations for spring. In each of the two categories of magnetic disturbance, the average *Kp* values were 1.7 and 3.9, the average 10.7-cm solar flux indices were 155 and 169, and the number of independent velocities were 62634 and 53797, respectively. The drifts during spring showed features in common to both autumn and winter. For example, the behaviour of $V_{\perp S}$ during spring and autumn was similar, but there was evidence for enhanced poleward motion near sunrise (∼04–07 h) in spring. This enhancement still occurred even when the vertical component of motion was set to zero, prior to transforming the velocities into the magnetic reference frame; hence, it was not an artefact associated with photo-production at sunrise. Buonsanto and Witasse (1999) also reported some unexplained peaks in poleward drift during ∼03–06 h in Millstone Hill measurements. We speculate that the enhanced poleward drift at Bundoora may indicate a significant zonal electric field setup by the sharp conductivity gradient across the sunrise terminator.

The behaviour of $V_{\perp E}$ during spring resembled the behaviour during autumn, with eastward enhancements near ∼07 h, 10 h, and a subdued enhancement near ∼16 h. However, the perturbations in $V_{\perp E}$ were more winter-like, but with weaker amplitudes. The differences between autumn and spring may be partly accounted for by the differences in solar flux levels.

The preceding seasonal averages may not represent true long-term underlying averages since few geomagnetic storms occurred during each season. Hence, Fig. 7 shows the diurnal averages calculated using data recorded during all seasons. As expected, the meridional drifts and their perturbations were generally lower in amplitude than the corresponding zonal drifts (note the change of scales). The meridional perturbations had an average across all LST of

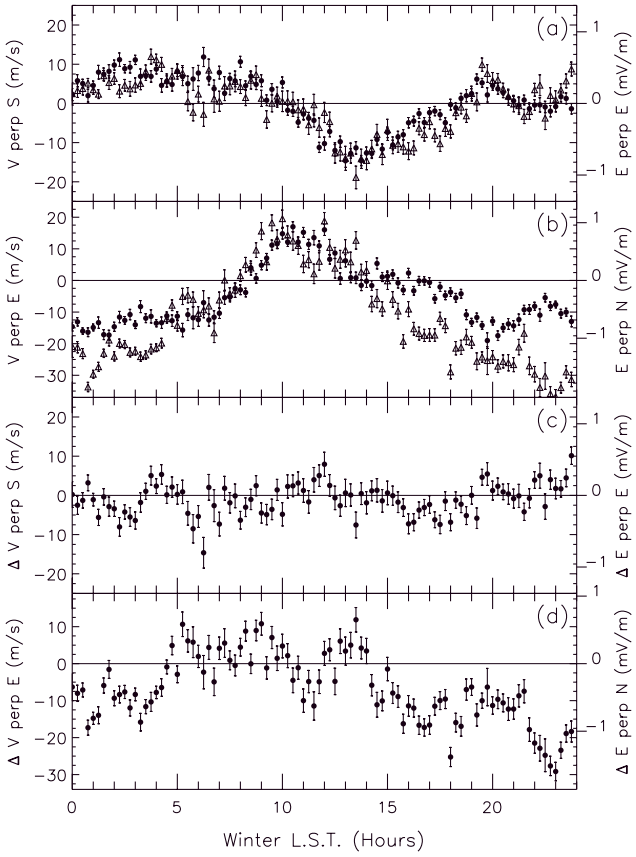


**Fig. 5.** The same results as Fig. 3 except for winter.

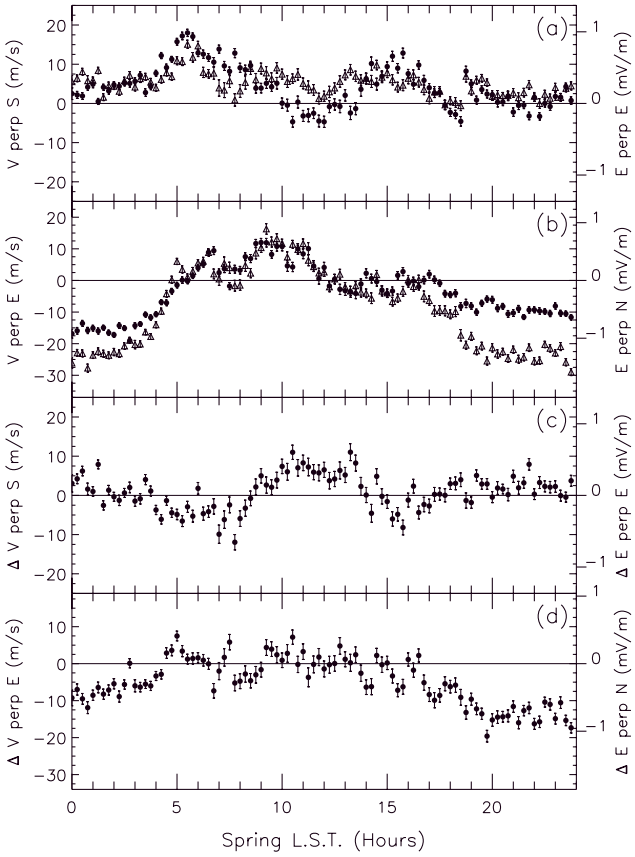


**Fig. 6.** The same results as Fig. 3 except for spring.

2.0 m s$^{-1}$, whereas the zonal perturbations had an average across all LST of −7.5 m s$^{-1}$, with this number decreasing to −14.0 m s$^{-1}$ when using the more selective categories $Kp < 2$ and $Kp > 4$. The zonal perturbations were distinctly westward during the afternoon, evening, and early morning (∼14–04 h), and distinctly eastward during the morning (∼05–11 h). This behaviour was most prevalent during winter and spring.

Now we investigate the dependence of the perturbation drifts on LST and *Kp* in greater detail. Figure 8 plots the average meridional drift $V_{\perp S}$ versus the *Kp* index for four-hourly intervals of LST. An average velocity, for say $Kp = 2$, actually means the average velocity recorded during all seasons when *Kp* was 2−, 2, or 2+. All the velocities recorded when *Kp* was >6− were lumped into a single, highly disturbed "$Kp = 6$" category. Otherwise, the high *Kp* values would have had very large error bars since there were few geomagnetic storms of this magnitude. The heavy black curve shows the weighted diurnal averages across all LST. Considering the results of Figs. 3 to 7, it is not surprising that the average perturbations in $V_{\perp S}$, shown in Fig. 8, are weak (<10 m s$^{-1}$) and wildly fluctuating. Nonetheless, $V_{\perp S}$ results are shown because they illustrate how difficult it is for zonal electric fields of magnetospheric origin to penetrate to mid-latitudes.

Figure 9 shows the same results as Fig. 8, except for the more clearly defined zonal drifts, $V_{\perp E}$. During the morning interval 08–12 h LST (small dots), the zonal drifts were ∼9 m s$^{-1}$ eastward over the entire *Kp* range 0 to >6−. However, we note that these are only average perturbation drifts, and they do not separate out the prompt penetration and longer-lasting disturbance dynamo contributions. For example, an examination of Bundoora measurements revealed an impulsive increase in velocity of >100 m s$^{-1}$ shortly after a large, sudden change in the interplanetary magnetic field (Parkinson et al., 2000). For all the 4 h intervals in the range 12–04 h, the drifts became increasingly westward over the *Kp* range 0 to >6−. The strongest westward perturbations occurred during the interval 20–24 h (crosses), with the perturbations often much less than 30 m s$^{-1}$ for $Kp > 6-$.

If the data points for $Kp > 6-$ had been included in Fig. 9 separately, the behaviour of the curves would become very erratic. Although this is partly due to the small number of samples, it is probably also a consequence of the mid-latitude trough and the high-latitude convection zone expanding equatorward to the latitude of Bundoora (Parkinson et al., 1996).

## 5 Further discussion

Overall, the drifts at Bundoora have far more in common with ISR results for Millstone Hill (71.5° W, 42.6° N, geo-

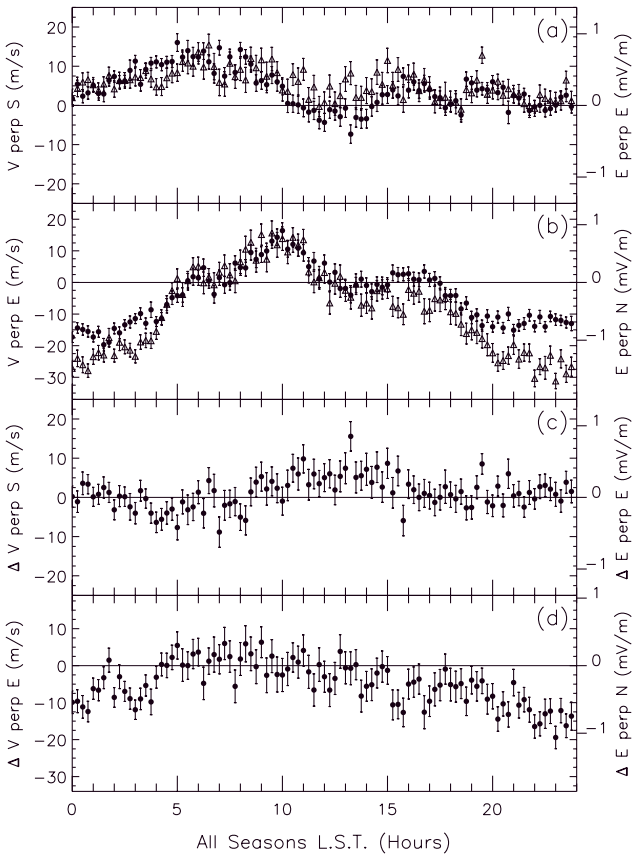


**Fig. 7.** The same results as Fig. 3 except for all seasons combined.

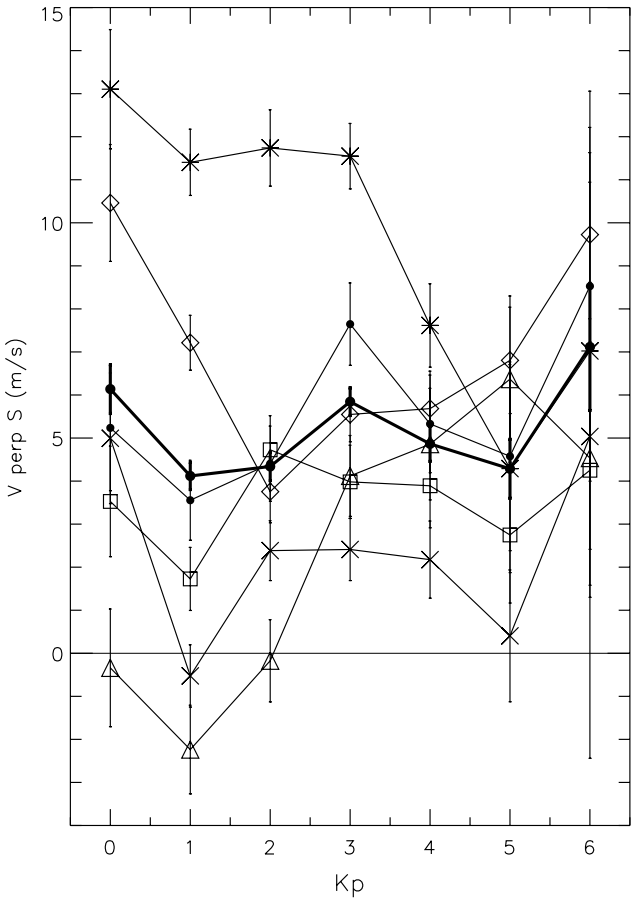


**Fig. 8.** The dependence of $V_{\perp S}$ on the *Kp* index for different 4-h intervals of LST: 00–04 h (diamonds), 04–08 (asterisks), 08–12 (small dots), 12–16 (triangles), 16–20 (squares), and 20–24 (crosses). The heavy black line is the weighted average across all intervals of LST. Error bars are standard deviations of the mean.

graphic; 57° N magnetic) than Saint Santin (2.2° E, 44.6° N; 40° N) (Blanc and Amayenc, 1979; Blanc, 1983; Buonsanto and Witasse, 1999; Scherliess et al., 2000). However, there is some agreement between the meridional drifts measured at Bundoora and Saint Santin. For example, observations at both stations show an equatorward excursion of the drifts near local noon. On the other hand, the Saint Santin zonal drifts are mostly westward during 0–13 h and eastward during 13–24 h LST. This contrasts with the Bundoora zonal drifts which tend to be eastward only briefly during the late morning.

Numerous studies have analysed Millstone Hill drift data and obtained similar results. For example, we have compared our results shown in Figs. 3–7 with the Millstone Hill results shown in Fig. 1 of Wand and Evans (1981c). The quiet zonal drifts observed at both stations show well-defined westward motions during the nighttime. This might be considered surprising given the wide geographic separation of the two stations. However, the midday peak in eastward drift occurs several hours earlier at Bundoora. The agreement with the westward perturbation drifts, especially during the pre-midnight hours, is excellent. Subauroral ion drift events (SAIDs; see Anderson et al., 1991) are also known to have peak westward flows in the pre-midnight hours. Hence, the relationship between SAIDs and the mid-latitude westward drifts, observed here, requires further investigation.

We have also compared the meridional drifts for Bundoora with those for Millstone Hill, as shown in Fig. 1 of Buonsanto et al. (1993). There is some agreement between the meridional drifts observed at the two stations, especially during the austral winter. Again, observations at both stations show an equatorward excursion of the drifts near local noon. However, the agreement with the zonal drifts is better than for the weaker meridional drifts, and suggests there may be greater longitudinal structure in the meridional drifts than the zonal drifts. Of course, any differences between the electric fields at Bundoora and Millstone Hill are probably related to the wide longitudinal (and small latitudinal) separation of the two stations, as well as the consequences of the different geomagnetic dipole tilts.

Assuming the ionospheric drifts measured by the Digisonde correspond to true plasma drifts and not the effects of gravity waves or production and loss processes, what causes the seasonal variations in the observed drifts? For example, why were there differences between the summer and winter drifts? If the Earth's geomagnetic dipole field were closely aligned with the rotational axis, then large differences be-

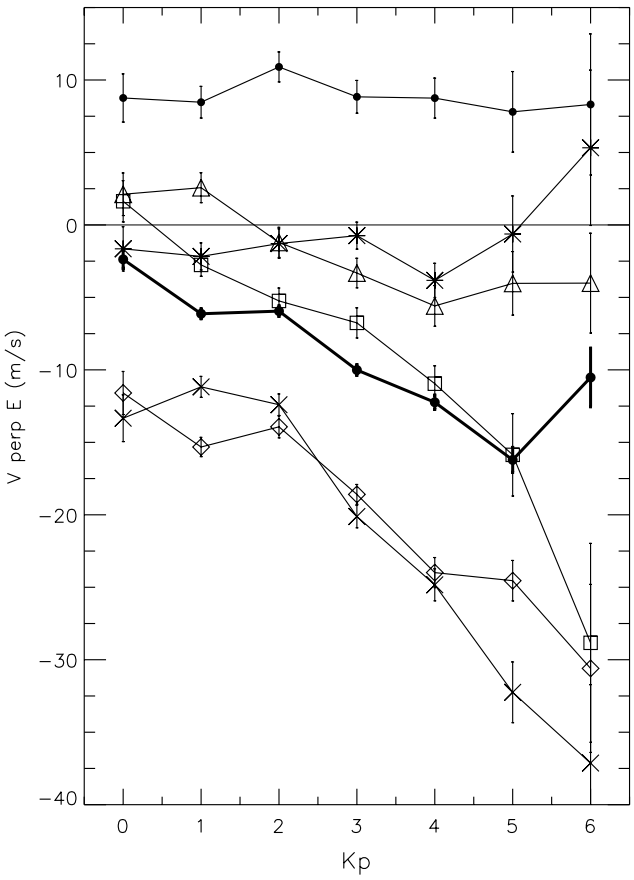


**Fig. 9.** The same as Fig. 8 except for $V_{\perp E}$. The results are given for the same 4-h intervals of LST: 00–04 h (diamonds), 04–08 (asterisks), 08–12 (small dots), 12–16 (triangles), 16–20 (squares), and 20–24 (crosses).

tween summer and winter drifts would not occur because the same electric fields would map along the flux tube connecting regions of seasonally symmetric conductivity, i.e. the E-region conductivity in the Southern Hemisphere during austral summer would be the same as in the Northern Hemisphere during the boreal summer. The same can be said for the winters.

The tilt of the geomagnetic dipole field means that Bundoora (145.1° E, 37.7° S geographic) has a conjugate point in the Sea of Okhotsk (OKH) (154.0° E, 55.4° N). Hence, at austral summer solstice, the sub-solar point at noon is 14° away from Bundoora and 79° away from OKH, whereas at winter solstice, the sub-solar point is 61° away from Bundoora and 32° away from OKH. Consequently, during austral summer, the very high E-region conductivity above Bundoora is mapped to a region of very low conductivity. In contrast, during austral winter, the moderate conductivity above Bundoora is mapped to a region of high conductivity. The seasonal behaviour of winds in the lower thermosphere at the different geographic (but magnetically conjugate) regions will also be different at the same time of year.

Some other interesting effects might also occur at sunrise because the station in the summer hemisphere will cross the terminator before the station in the winter hemisphere. Similar explanations were invoked by Fejer (1993) and Takami et al. (1996) to explain the observed similarity between drifts measured above Arecibo during summer and above Shigaraki during winter (and vice versa). Obviously there is wide scope for changes in the seasonal variations of electric fields above a particular station, but the actual importance of different mechanisms requires a detailed comparison between models and measurements.

## 6 Summary and conclusions

Figure 7 summarised the behaviour of F-region Doppler velocity measured by the Digisonde at Bundoora (145.1° E, 37.7° S geographic; 49° S geomagnetic). The meridional drifts were basically poleward during ∼00–10 h, 15–17 h, and 19–21 h LST, and equatorward during ∼10–14 h. A poleward enhancement was pronounced in spring near sunrise, ∼04–07 h. Meridional drifts and their perturbations tended to be weaker than the zonal drifts. They also exhibited a more erratic diurnal structure. The zonal drifts and their perturbations tended to be westward during ∼00–05 h and 13–24 h, and weakly eastward during ∼05–11 h. The strongest perturbation drifts were westward during the night, 18–04 h, and increased in magnitude with *Kp* over the range 0 to >6−, but were confused for very high values of *Kp*, partly because of the equatorward expansion of the magnetospheric convection zone.

As of yet, our database is not sufficiently large to investigate solar flux dependencies. However, we found significant seasonal changes in the drift variations measured above Bundoora. The seasonal changes were probably caused by changes in the lower thermospheric winds, combined with the consequences of the geomagnetic dipole tilt, i.e. there were differences in the ionospheric conductivity and tides regulating the quiet time and disturbance dynamos at Bundoora and its conjugate location. We might expect the seasonal changes to be larger for Bundoora than many other stations because of the large displacement of the geomagnetic pole toward the station.

Overall, our results show that meridional electric fields (i.e. zonal drifts) of magnetospheric origins are more likely to penetrate to mid-latitudes than zonal electric fields (i.e. meridional drifts). The westward drifts and their perturbations measured with the Digisonde at Bundoora resemble those measured by the ISR at Millstone Hill. Moreover, the westward perturbations are a global feature seen in DE-2 ion drift measurements (Fejer and Scherliess, 1998). Hence, the good agreement between the westward perturbation drifts measured using these different techniques is a “smoking gun”, indicating that all instruments, including our average Digisonde velocities, do correspond to true ion motions driven by ionospheric electric fields. However, we emphasise caution because production and loss processes and the passage of gravity waves must often modulate the

AOA and Doppler shift of reflection surfaces in the radar's field of view. More common volume comparisons between Digisonde, ISR, and HF backscatter radar measurements are required to determine whether the Digisonde velocities can be used to reliably infer electric fields at mid-latitudes on time scales $<3$ h. An ideal experiment would be to compare Digisonde measurements made at magnetically conjugate locations since observations of similar velocities would imply they were driven by the same electric field mapping along the magnetic flux tube.

Nevertheless, the results of the present study suggest that with sufficient averaging, Doppler velocities measured with digital ionosondes at mid-latitudes correspond to true F-region ion motion. Our results must help to improve the ionospheric modelling effort by providing data from the Southern Hemisphere, a region of the mid-latitude ionosphere with relatively few electric field measurements.

*Acknowledgements.* This work was supported by the Australian Research Council and RLM Systems Pty. Ltd. We thank all those people who helped to install and maintain the Bundoora Digisonde including C. Buratto, L. Chong, E. Huwald, R. Lepping, B. Lobb, M. Mulready, K. W. Ogilvie, and W. Trapp. K. Cole is thanked for his insightful comments. We also thank the Australian Spectrum Management Agency for allowing us to perform these experiments.

Topical Editor M. Lester thanks R. Stening and P. S. Cannon for their help in evaluating this paper.

## References

Anderson, P. C., Heelis, R. A., and Hanson, W. B., The ionospheric signatures of rapid subauroral ion drifts, J. Geophys. Res., 96, 5785–5792, 1991.

Behnke, R. A. and Harper, R. M., Vector measurements of F region ion transport at Arecibo, J. Geophys. Res., 78, 8222–8234, 1973.

Bittencourt, J. A. and Abdu, M. A., A theoretical comparison between apparent and real vertical ionization drift velocities in the equatorial F region, J. Geophys. Res., 86, 2451–2454, 1981.

Blanc, M., Magnetospheric convection at mid-latitudes 3. Theoretical derivation of the disturbance convection pattern in the plasmasphere, J. Geophys. Res., 88, 235–251, 1983.

Blanc, M. and Amayenc, P., Seasonal variation of the ionospheric $\boldsymbol{E} \times \boldsymbol{B}$ drifts, J. Geophys. Res., 84, 2691–2704, 1979.

Buonsanto, M. J., Hagan, M. E., Salah, J. E., and Fejer, B., Solar cycle and seasonal variations in F region electrodynamics at Millstone Hill, J. Geophys. Res., 98, 15677–15683, 1993.

Buonsanto, M. J. and Witasse, O. G., An updated climatology of thermospheric neutral winds and F region ion drifts above Millstone Hill, J. Geophys. Res., 104, 24675–24687, 1999.

Cannon, P. S., Reinisch, B. W., Buchau, J., and Bullett, T. W., Response of the polar cap F region convection direction to changes in the interplanetary magnetic field: Digisonde measurements in northern Greenland, J. Geophys. Res., 96, 1239–1250, 1991.

Dyson, P. L., Davies, T. P., Parkinson, M. L., Reeves, A. J., Richards, P. G., and Fairchild, C. E., Thermospheric neutral winds at southern mid-latitudes: A comparison of optical and ionosonde *hm*F2 methods, J. Geophys. Res., 102, 27189–27196, 1997.

Du, J. and Stening, R. J., Simulating the ionospheric dynamo – I. Simulation model and flux tube integrated conductivities, J. Atmos. Solar-Terr. Phys., 61, 913–923, 1999a.

Du, J. and Stening, R. J., Simulating the ionospheric dynamo – II. Equatorial Electric fields, J. Atmos. Solar-Terr. Phys., 61, 925–940, 1999b.

Fejer, B. G., F region plasma drifts over Arecibo: solar cycle, seasonal, and magnetic activity effects, J. Geophys. Res., 98, 13645–13652, 1993.

Fejer, B. G., The electrodynamics of the low-latitude ionosphere: recent results and future challenges, J. Atmos. Solar-Terr. Phys., 59, 1465–1482, 1997.

Fejer, B. G. and Scherliess, L., Mid- and low-latitude prompt-penetration ionospheric zonal plasma drifts, Geophys. Res. Lett., 25, 3071–3074, 1998.

From, W. R., Sadler, E. M., and Whitehead, J. D., Measuring ionospheric movements using totally reflected radio waves, J. Atmos. Terr. Phys., 50, 153–165, 1988.

Grant, I. F. et al., Comparison of plasma flow velocities determined by ionosonde Doppler drift technique, SuperDARN radars, and patch motion, Radio Sci., 30, 1537, 1995.

Haines, D. M. and Reinisch, B. W., Digisonde Portable Sounder System Manual, Univ. of Mass., Lowell Cent. for Atmos. Res., 1995.

Heelis, R. A. and Coley, W. R., East-west ion drifts at mid-latitudes observed by Dynamics Explorer 2, J. Geophys. Res., 97, 19461–19469, 1992.

Heppner, J. P. and Maynard, N. C., Empirical high-latitude electric field models, J. Geophys. Res., 92, 4467–4489, 1987.

Jarvis, M. J., Jenkins, B., and Rodgers, G. A., Southern hemisphere observations of a long-term decrease in F region altitude and thermospheric wind providing possible evidence for global thermospheric cooling, J. Geophys. Res., 103, 20774–20787, 1998.

Papitashvili, V. O., Belov, B. A., Faermark, D. S., Feldstein, Y. I., Golyshev, S. A., Gromova, L. I., and Levitin, V. E., Electric potential patterns in the northern and southern polar regions parameterized by the interplanetary magnetic field, J. Geophys. Res., 99, 12251–12262, 1994.

Parkinson, M. L., Dyson, P. L., and Quach, A. T. D., Arrival of ionospheric troughs and oblique spread-F in the wake of large-scale travelling ionospheric disturbances during the intense auroral storms of August 22 and 23, 1990, J. Geomag. Geoelect., 48, 1381–1405, 1996.

Parkinson, M. L., Dyson, P. L., and Smith, P. R., Analysis of direction-of-arrival aliasing for MF/HF Doppler-sorted interferometry measurements of ionospheric drift, Radio Sci., 32, 999–1009, 1997a.

Parkinson, M. L., Monselesan, D. P., Smith, P. R., Dyson, P. L., and Morris, R. J., Digital ionosonde measurements of the height variation of drift velocity in the southern polar cap ionosphere: initial results, J. Geophys. Res., 102, 24075–24090, 1997b.

Parkinson, M. L., Breed, A. M., Dyson, P. L., and Morris, R. J., Application of the Dopplionogram to Doppler-sorted interferometry measurements of ionospheric drift velocity, Radio Sci., 34, 899–912, 1999.

Parkinson, M. L., Polglase, R., Dyson, P. L., Fejer, B. G., Scherliess, L., and Ujmaia, S. M., Electric field measurements at a southern mid-latitude station obtained using an HF digital ionosonde, Adv. Space Res., in press, 2001.

Reinisch, B. W., New techniques in ground-based ionospheric sounding and studies, Radio Sci., 21, 331–341, 1986.

Reinisch, B. W., Haines, D. M., Bibl, K., Galkin, I., Huang, X., Kitrosser, D. F., Sales, G. S., and Scali, J. L., Ionospheric sound-

ing in support of over-the-horizon radar, Radio Sci., 32, 1681–1694, 1997.

Richmond, A. D., Ionospheric Electrodynamics, in Handbook of Atmospheric Electrodynamics, Vol. 2, Ed. H. Volland, pp. 249–290, CRC Press, Boca Raton, 1995.

Roble, R. and Dickinson, R. E., How will changes in carbon dioxide and methane modify the mean structure of the mesosphere and thermosphere? Geophys. Res. Lett., 16, 1441–1444, 1989.

Saxton, J. M. et al., Quiet time plasmaspheric electric fields and plasmasphere-ionosphere coupling fluxes at $L = 2.5$, Planet. Space Sci., 37, 283–293, 1989.

Scali, J. L., Reinisch, B. W., Heinselman, C. J., and Bullett, T. W., Coordinated digisonde and incoherent scatter radar F region drift measurements at Sondre Stromfjord, J. Geophys. Res., 30, 1481–1498, 1995.

Scali, J., Reinisch, B., Dozois, C., Bibl, K., Kitrosser, D., Haines, M., and Bullett, T., Digisonde Drift Analysis, University of Massachusetts, Lowell Center for Atmospheric Research, 1995b.

Scali, J. L., Reinisch, B. W., Kelley, M. C., Miller, C. A., Swartz, W. E., Zhou, Q. H., and Radicella, S., Incoherent scatter radar and Digisonde observations at tropical latitudes, including conjugate point studies, J. Geophys. Res., 102, 7357–7367, 1997.

Scherliess, L. and Fejer, B. G., Satellite studies of mid- and low-latitude ionospheric disturbance zonal plasma drifts, Geophys. Res. Lett., 25, 1503–1506, 1998.

Scherliess, L., Fejer, B. G., Holt, J., Goncharenko, L., Amory-Mazaudier, C., and Buonsanto, M. J., Radar studies of mid-latitude ionospheric plasma drifts, J. Geophys. Res., submitted, 2000.

Smith, P. R., Dyson, P. L., Monselesan, D. P., and Morris, R. J., Ionospheric convection at Casey, a southern polar cap station, J. Geophys. Res., 103, 2209–2218, 1998.

Takami, T., Oliver, W. L., Richmond, A. D., and Fukao, S., Ionospheric drift similarities at magnetic conjugate locations, J. Geophys. Res., 101, 15773–15782, 1996.

Wand, R. H., A model representation of the ionospheric electric field over Millstone Hill ($\Lambda = 56°$), J. Geophys. Res., 86, 5801–5808, 1981.

Wand, R. H. and Evans, J. V., Seasonal and magnetic activity variations of ionospheric electric fields over Millstone Hill, J. Geophys. Res., 86, 103–118, 1981a.

Wand, R. H. and Evans, J. V., The penetration of convection electric fields to the latitude of Millstone Hill ($\Lambda = 56°$), J. Geophys. Res., 86, 5809–5814, 1981b.

Weimer, D. R., A flexible, IMF dependent model of high-latitude electric potentials having “space weather” applications, Geophys. Res. Lett., 23, 2549–2552, 1996.

Wright, J. W. and Pitteway, M. L. V., High-resolution vector velocity determinations from the Dynasonde, J. Atmos. Solar-Terr. Phys., 56, 961–977, 1994.